THE JOURNAL OF BIOLOGICAL CHEMISTRY
Vol. 275, No. 45, Issue of November 10, pp. 35335–35344, 2000
Printed in U.S.A.

Novel ω-Conotoxins from *Conus catus* Discriminate among Neuronal Calcium Channel Subtypes*

Received for publication, March 17, 2000, and in revised form, July 5, 2000
Published, JBC Papers in Press, August 8, 2000, DOI 10.1074/jbc.M002252200

Richard J. Lewis‡§¶‖, Katherine J. Nielsen‡, David J. Craik‡, Marion L. Loughnan‡, Denise A. Adams‡, Iain A. Sharpe‡§, Tudor Luchian‡§, David J. Adams§, Trudy Bond‡, Linda Thomas‡, Alun Jones‡, Jodi-Lea Matheson‡‡§§, Roger Drinkwater‡‡§§, Peter R. Andrews‡, and Paul F. Alewood‡**

From the ‡Centre for Drug Design and Development (3D Centre), Institute for Molecular Bioscience, §Department of Physiology and Pharmacology, ‡‡CSIRO Tropical Agriculture, and ¶Queensland Agricultural Biotechnology Centre (QDPI), The University of Queensland, Brisbane, Queensland 4072, Australia

ω-Conotoxins selective for N-type calcium channels are useful in the management of severe pain. In an attempt to expand the therapeutic potential of this class, four new ω-conotoxins (CVIA–D) have been discovered in the venom of the piscivorous cone snail, *Conus catus*, using assay-guided fractionation and gene cloning. Compared with other ω-conotoxins, CVID has a novel loop 4 sequence and the highest selectivity for N-type over P/Q-type calcium channels in radioligand binding assays. CVIA–D also inhibited contractions of electrically stimulated rat vas deferens. In electrophysiological studies, ω-conotoxins CVID and MVIIA had similar potencies to inhibit current through central ($\alpha_{1B\text{-}d}$) and peripheral ($\alpha_{1B\text{-}b}$) splice variants of the rat N-type calcium channels when coexpressed with rat β_3 in *Xenopus* oocytes. However, the potency of CVID and MVIIA increased when $\alpha_{1B\text{-}d}$ and $\alpha_{1B\text{-}b}$ were expressed in the absence of rat β_3, an effect most pronounced for CVID at $\alpha_{1B\text{-}d}$ (up to 540-fold) and least pronounced for MVIIA at $\alpha_{1B\text{-}d}$ (3-fold). The novel selectivity of CVID may have therapeutic implications. ^{1}H NMR studies reveal that CVID possesses a combination of unique structural features, including two hydrogen bonds that stabilize loop 2 and place loop 2 proximal to loop 4, creating a globular surface that is rigid and well defined.

Predatory marine gastropods of the genus *Conus* (cone snails) represent a diverse family of marine molluscs that use venom for prey capture. The venom of each species contains a unique array of more than 100 peptides, whose pharmaceutical potential remain largely unexploited (1). Different classes of conotoxins have evolved to target ion channels and receptors for the successful capture of fish, molluscs, or worms (2, 3). One important class, the ω-conotoxins (Table I) isolated from piscivorous species, inhibits neuronal voltage-sensitive calcium channels (VSCCs)[1] found in mammals (4). ω-Conotoxins have selectivity for N-type (*e.g.* MVIIA and GVIA) or P/Q-type (*e.g.* MVIIC) VSCCs, making them widely used research tools for defining the distribution and role of neuronal VSCCs (4–8). In addition to their use as research tools, animal studies have shown that ω-conotoxins that target N-type VSCCs have clinical potential in ischemic brain injury (9) and pain (10). However, ω-conotoxins presently available are not ideal therapeutics, despite their selectivity and potency and the dominant role of N-type VSCCs at synapses in carrying nociceptive information in the spinal cord (11). For example, intrathecal MVIIA causes a variety of neurological side effects of unknown origin (12). Another N-type VSSC selective ω-conotoxin, GVIA, dissociates slowly from N-type VSCCs (13, 14) and, accordingly, may be difficult to administer in a clinical setting. Other ω-conotoxins are less selective for N-type VSCCs and are not considered useful therapeutic candidates.

A number of central and peripheral splice variants of the N-type VSCC have been reported (14). However, calcium channel probes with greater selectivity are required to help understand the role(s) played by the various forms of the N-type VSCC in normal and disease states. Here we report the isolation and characterization of four new ω-conotoxins (CVIA—D, see Table I) discovered in the venom of the piscivorous cone snail, *Conus catus*. One of these, CVID, has a number of novel structural features that underlie an enhanced ability to discriminate between N-type (α_{1B}) and P/Q-type (α_{1A}) VSCCs, as well as between splice variants of the α_{1B} expressed in oocytes in the presence or absence of rat β_3.

EXPERIMENTAL PROCEDURES

Crude Venom Extraction—37 specimens of *C. catus* (average length 4 cm) were collected from the southern Great Barrier Reef. Crude venom duct contents were extracted with 30% acetonitrile/water acidified with 0.1% trifluoroacetic acid and centrifuged. Soluble material was lyophilized and stored at −20 °C prior to use.

Isolation of Native Peptides—The crude venom extract (12 mg) was fractionated using semi-preparative RP-HPLC (10 μm C18, 1.0 × 25 cm, Vydac) eluted at 2.5 ml/min with a linear gradient of 0–60% solvent B over 60 min, then to 80% solvent B over 20 min, using a Waters 600 solvent delivery system (solvent A, 10% acetonitrile, 0.1% trifluoroacetic acid; solvent B, 90% acetonitrile, 0.09% trifluoroacetic acid). Inhibition of ^{125}I-GVIA binding to rat brain membrane (see below) identified six 1-min fractions eluting at 17, 18, 22, 23, 26, and 27 min that contained ω-conotoxins. The ω-conotoxins in each fraction were further

* This work was supported by a grant from AusIndustry provided under the Generic Technology component of the Industry Research and Development Act, 1986, and AMRAD Operations Pty Ltd. The costs of publication of this article were defrayed in part by the payment of page charges. This article must therefore be hereby marked "*advertisement*" in accordance with 18 U.S.C. Section 1734 solely to indicate this fact.

‖ To whom correspondence should be addressed: Centre for Drug Design and Development, Inst. for Molecular Bioscience, The University of Queensland, Brisbane 4072, Australia. Fax: 61-7-3365-1990; E-mail: r.lewis@mailbox.uq.edu.au.
** Australian Research Council senior fellow.
§§ Current address: Xenome Ltd., 50 Meiers Rd., Indooroopilly, Queensland 4608, Australia.

[1] The abbreviations used are: VSCCs, voltage-sensitive calcium channels; RP-HPLC, reverse phase-high pressure liquid chromatography; PCR, polymerase chain reaction; ds, double-stranded; MS, mass spectrometer; NOE, nuclear Overhauser effect.

TABLE I
Sequence and VSCC selectivity of selected ω-conotoxins

Name[a]	Sequence[b]	Selectivity[c]	Ref.
Loop	1 2 3 4		
CVIA	**C**KSTGAS**C**RRTSYD**CC**TGS**C**RS--GR**C***	N	Present study
CVIB	**C**KGKGAS**C**RKTMYD**CC**RGS**C**RS--GR**C***	N/P/Q	Present study
CVIC	**C**KGKGQS**C**SKLMYD**CC**TGS**C**SRR-GK**C***	N/P/Q	Present study
CVID	**C**KSKGAK**C**SKLMYD**CC**SGS**C**SGTVGR**C***	N	Present study
GVIA	**C**KSOGSS**C**SOTSYN**CC**R-S**C**NOYTKR**C**Y*	N	57
TVIA	**C**LSOGSS**C**SOTSYN**CC**R-S**C**NOYSRK**C**Y*	N	4
MVIIA	**C**KGKGAK**C**SRLMYD**CC**TGS**C**RS--GK**C***	N	58
MVIIC	**C**KGKGAP**C**RKTMYD**CC**SGS**C**GRR-GKC*	P/Q	59
SVIB	**C**KLKGQS**C**RKTSYD**CC**SGS**C**GRS-GK**C***	N/P/Q	51

[a] ω-Conotoxins from the venom of piscivorous *C. catus* (C), *C. geographus* (G), *C. tulipa* (T), *C. magus* (M), and *C. striatus* (S) are shown.
[b] All ω-conotoxins are C-terminally amidated (*).
[c] Selectivity determined from relative potencies to displace ^{125}I-GVIA (N-type) and ^{125}I-MVIIC (P/Q-type) binding to rat brain membrane.

purified by size exclusion HPLC (Superdex HR10/30, Amersham Pharmacia Biotech) eluted with 30% acetonitrile, 0.1% trifluoroacetic acid at 0.5 ml/min. Active fractions were finally rechromatographed by analytical RP-HPLC (5 μm C18, 0.46 × 25 cm, Vydac) eluted at 1 ml/min with a linear gradient of 0–50% solvent B over 45 or 90 min. Peaks detected at 214 nm were collected and sequenced. Screening of the venom of other Australian cone snails, including the piscivorous *Conus striatus, Conus tulipa, Conus geographus*, and *Conus magus*, only identified sequences corresponding to known ω-conotoxins.

Sequencing of Native Peptides—The purified peptides (~100 pmol) were reduced in the presence of TCEP, 50 mM ammonium acetate at pH 4.5 (37 °C for 1 h), and then alkylated in the presence of maleimide (37 °C, 1 h). The alkylated peptides were purified by RP-HPLC, applied to a Biobrene-treated glass fiber filter, and analyzed by Edman chemistry using an Applied Biosystems, Inc., model 470A protein sequencer. Alkylation of peptides with maleimide allowed their cysteine residues to be observed as phenylthiohydantoin-Cys-maleimide doublets (diastereomers), and Ser was confirmed by the presence of dehydroserine. The high number of serine, threonine, and cysteine residues present in each conotoxin resulted in a relatively rapid decrease in the amino acid yields in successive cycles; however, complete sequences were obtained in each case. The low serine signals were accompanied by the presence of large dehydroserine peak.

Gene Isolation and Characterization—Ducts from two specimens of *C. catus* were emulsified, and poly(A)$^+$-tailed mRNA was extracted using the QuickPrep mRNA purification system (Amersham Pharmacia Biotech). Strand-1 cDNA was 3′ end-synthesized from the *C. catus* poly(A)$^+$ mRNA templates using a *Not*I-d(T)$_{18}$ bifunctional primer (5′-AACTGGAAGAATTCGCGGCCGCAGGAAT$_{18}$) (Amersham Pharmacia Biotech) extended with Superscript II reverse transcriptase (Life Technologies, Inc.). The resultant cDNA templates were used to manufacture double-stranded cDNA using a RNase H/DNA polymerase procedure (cDNA Timesaver system, Amersham Pharmacia Biotech). Marathon adaptors (CLONTECH) were added to the 5′ and 3′ ends of the ds-cDNA molecules to complete the cDNA construction. An oligonucleotide PCR primer (R-301A 5′-atcatcaaaATGAAACTGACGTG) was designed from a consensus of aligned coding sequences from conotoxins with a 6-cysteine/4-loop framework comprising published (15, 16) and unpublished data.[2] The primer included a translation start site (underlined) and 9 base pairs of 5′-untranslated sequence (lowercase). This forward PCR primer was designed to work in conjunction with the reverse ANCHOR primer (5′- AACTGGAAGAATTCGCGGCCGCAGGAAT) that was homologous to the adaptor at the 3′ termini of the ds-cDNA templates.

PCR was carried out on samples containing ds-cDNA from *C. catus*, the R-301A primer, the ANCHOR primer, AmpliTaq Gold polymerase (PerkinElmer Life Sciences), the manufacturer's AmpliTaq buffer, 25 mM $MgCl_2$, and 100 μM deoxynucleotides. The samples were incubated in a PTC-100 thermal cycler (MJ Research, Bresatec, Australia) at 95 °C for 2 min (1 cycle), 95 °C for 30 s, 55 °C for 60 s, 72 °C for 90 s (35 cycles), and 72 °C for 10 min (1 cycle). The PCR products were assessed on agarose gels and, when necessary, isolated and purified using BRESAspin gel extraction systems (Bresatec, Australia). The purified PCR products were blunt end-cloned into dephosphorylated *Sma-1* cut pUC-18 plasmid vector DNA (Amersham Pharmacia Biotech) and sequenced using the pUC-18 forward and reverse primers (Amersham Pharmacia Biotech), dideoxy terminator sequencing chemistries (PerkinElmer Life Sciences) on Applied Biosystems, Inc., 377 sequencers.

Peptide Synthesis—CVIA–D were each manually synthesized, deprotected, and cleaved from resin as described previously (17, 18). *O*-(7-Azabenzotriazol-1-yl)-*N,N,N′,N′*-tetramethyluronium hexafluorophosphate was used in place of *O*-(benzotriazol-1-yl)-*N,N,N′,N′*-tetramethyluronium hexafluorophosphate for difficult sections. The pure, reduced peptides (0.02–0.05 mM) were oxidized in aqueous 0.33 M NH_4Oac, 0.5 M guanidine·HCl (pH 7.5–8.0, adjusted with 0.1 M NH_4OH). The peptide solutions were then stirred for 2–4 days at 4 °C in the presence of reduced and oxidized glutathione (molar ratio 1:100:10) to achieve oxidation. Oxidized peptides were purified by preparative RP-HPLC (18).

Peptide Quantitation—Peptides were quantified initially by triplicate amino acid analysis (19) and then by RP-HPLC (HP 1100) using an external reference standard for each peptide. Stability studies in physiological saline solutions showed that nonspecific binding of these peptides to glass or polypropylene was minimal.

Mass Spectrometry—Mass spectra were acquired on a PE-Sciex API III triple quadrupole electrospray mass spectrometer (MS) in positive ion mode (m/z 500–2000, at 0.1–0.2-Da steps, declustering potentials of 10–90 V, and dwell times of 0.4–1.0 s). Data were deconvoluted (MacSpec 3.2, Sciex, Canada) to obtain the molecular weight from the multiply charged species. MS was used to confirm purity and to monitor peptide oxidation. Native and synthetic CVIA–D were compared on a 5-μm C18 column (0.21 × 25 cm, Vydac) eluted with 0.05% trifluoroacetic acid for 2 min and then with a linear gradient to 80% solvent B (solvent B, 90% acetonitrile, 0.045% trifluoroacetic acid) over 80 min at a flow rate of 130 μl/min, using a Hewlett-Packard 1100 pump and MS detection.

Radioligand Binding—Radioligand binding were performed on rat brain membrane incubated in the following (mM): 20 HEPES (pH 7.2), 75 NaCl, 0.1 EDTA, 0.1 EGTA, 2 leupeptin, 0.5 units of aprotinin, and 0.1% bovine serum albumin, as described previously (18, 20, 21). ^{125}I-[Tyr^{22}]GVIA, ^{125}I-CVID, ^{125}I-MVIIA, and ^{125}I-MVIIC were prepared using IODOGEN, stored at 4 °C, and used within 3 weeks. ^{125}I-CVID and ^{125}I-MVIIA both eluted ~3 min after CVID or MVIA, respectively, as single homogenous peaks on RP-HPLC. Cold iodinated CVID (^{127}I-CVID) was also prepared and quantified by HPLC. ^{127}I-CVID coeluted with ^{125}I-CVID, and MS confirmed it as the monoiodinated species. For displacement studies, [^{125}I-Tyr^{22}]GVIA, ^{125}I-MVIIA, or ^{125}I-MVIIC (7 pM diluted with assay buffer) were incubated with increasing concentrations of cold peptide. Saturation binding studies were performed with freshly prepared ^{125}I-CVID and ^{125}I-MVIIA (n = 4 experiments). On-rate and off-rate experiments were performed at 23 °C in single 50-ml polypropylene tubes containing ^{125}I-CVID or ^{125}I-MVIIA (30 pM diluted with assay buffer). On-rate experiments commenced with the addition of rat brain membrane, and off-rate experiments commenced with the addition of excess CVID or MVIIA (10^{-7} M) following a 30-min incubation of rat brain membrane with ^{125}I-CVID or ^{125}I-MVIIA (30 pM), respectively. At defined intervals, aliquots (300 μl) were filtered (25-mm Whatman GF/B treated with 0.6% polyethyleneimine), and the filtrates were rapidly washed three times with ice-cold wash buffer. Nonlinear regressions were fitted to each experiment (n = 3 data points per experiment) with Prism software (GraphPad, San Diego, CA).

Rat Vas Deferens—Male Wistar rats (250–350 × g) were killed by

[2] R. J. Lewis, K. J. Nielsen, D. J. Craik, M. L. Loughnan, D. A. Adams, I. A. Sharpe, T. Luchian, D. J. Adams, T. Bond, L. Thomas, A. Jones, J.-L. Matheson, R. Drinkwater, P. R. Andrews, and P. F. Alewood, unpublished data.

cervical dislocation and exsanguinated. Prostatic halves of each vas deferens were mounted under 0.5 × *g* tension in 5-ml organ baths containing physiological solution containing the following (mM): 119 NaCl, 4.7 KCl, 1.17, $MgSO_4$, 1.18 KH_2PO_4, 25.0 $NaHCO_3$, 5.5 glucose, 2.5 $CaCl_2$, 0.026 EDTA, at 37 °C and bubbled with 5% CO_2 in O_2 (pH 7.4). After 45 min of equilibration, electrical field stimulation every 3 min (single 55 V, 0.1-ms duration pulses generated by a Grass S44 stimulator) were applied via two platinum-stimulating electrodes straddling the tissue. Isometric contractions were measured using a force transducer (F-60, Narco Bio-System) and recorded digitally on a Power Macintosh computer using Chart version 3.5.6/s software and a MacLab/8 s data acquisition system (ADInstruments, Australia) at a sampling frequency of 200 Hz. Evoked contractions were abolished by tetradotoxin (0.1 μM), indicating that they were of neurogenic origin. Conotoxins were added cumulatively at 18-min intervals, with allowance made for a small (0.16% /min) deterioration of the evoked response. CVID effect on ATP (3×10^{-3} M, Sigma) and norepinephrine (10^{-4} M, Sigma) responses in the bisected epididymal portion of the rat vas deferens was also determined. Dose-response data (means ± S.E.; $n = 5$) were analyzed using Prism software.

Oocyte Injection and Recording—Oocytes were surgically removed from mature *Xenopus laevis* frogs anesthetized by submersion in 0.1% ethyl *m*-aminobenzoate (MS 222). Stage V–VI oocytes were prepared for injection by dissociation in Ca^{2+}-free solution containing the following (mM): 96 NaCl, 2 KCl, 1 $MgCl_2$, 5 HEPES (pH 7.4), plus 1 mg/ml collagenase (Sigma, type I) for 1 h at room temperature. Oocytes, maintained in storage solution containing (mM) 96 NaCl, 2 KCl, 1 $CaCl_2$, 1 $MgCl_2$, 5 HEPES, 5 pyruvate, plus 50 μg/ml gentamicin (pH 7.4), were injected with 25–50 ng of total cRNA using a precision injector (Drummond "Nanojet") and incubated at 18 °C for 3–5 days. Injected cRNA obtained using an Ambion mMessage mMachine kit comprised rat brain peripheral ($\alpha_{1B\text{-}b}$) or central ($\alpha_{1B\text{-}d}$) subunits of the N-type VSCC expressed in the absence or presence (1:1 ratio) of the rat β_3 subunit provided by D. Lipscombe (12). Recordings were made in a nominally Ca^{2+}-free solution containing (mM) 85 tetraethylammonium, 5 $BaCl_2$, 5 KCl, 5 HEPES, adjusted to pH 7.4 with methanesulfonic acid perfused at a rate of ~10 ml/min. Depolarization-activated Ba^{2+} currents were recorded using a GeneClamp 500B two-electrode voltage clamp amplifier (Axon Instruments Inc., Foster City, CA) at room temperature (21–23 °C). Voltage and current electrodes were filled with 3 M KCl and had final resistances of 0.2–1.0 MΩ. VSCC currents in oocytes were evoked by a step depolarization to 0 mV from a holding potential of −80 mV using pClamp programs (Axon Instruments Inc). The linear membrane capacitative and leak currents were subtracted using a −P/4 pulse protocol. Membrane currents were sampled at 10 kHz and filtered at 2 kHz. Oocytes showing <15% change in peak current amplitude over a 10-min incubation period were used in these studies to avoid effects associated with current run down. Oocytes that exhibited a slowly developing Cl^- current were discarded, and in control experiments on the remaining oocytes, BAPTA injection did not affect the Ba^{2+} current, indicating that this current was not contaminated by Ca^{2+}-activated Cl^- current. Perfusion was stopped, and cumulative additions of ω-conotoxins were added to a Teflon chamber (0.8 ml volume) to achieve rapid mixing. Inhibition of peak Ba^{2+} current amplitude was measured when the inhibitory effects of each concentration of MVIIA and CVID approached steady state values, typically requiring a 5–7-min incubation to achieve <2% change in peak current amplitude per min. Data (means ± S.E.; $n = 3$–5) were fitted with nonlinear regressions using Origin software.

^{1}H NMR and Three-dimensional Structure Calculations—All NMR experiments were recorded on a Bruker ARX 500 spectrometer equipped with a *z*-gradient unit, or a Bruker DMX 750 spectrometer equipped with an *x,y,z*-gradient unit. The Hα chemical shifts were obtained from spectra of CVIA–D in 95% H_2O, 5% D_2O (pH 2.5–3.5) at 293 K, and restraints for three-dimensional structure calculations of CVID were obtained from spectra recorded at 280 and 293 K at pH 3 and 5.5 (18). Structures were calculated using the torsion angle dynamics/simulated annealing protocol in XPLOR version 3.8 (22–25), as described previously (20).

RESULTS

Isolation and Synthesis of ω-Conotoxins from C. catus—The four ω-conotoxins, CVIA–D, were isolated from the crude venom of *C. catus* using activity-directed fractionation. Each comprised <1% of total venom peptide as determined by HPLC (214 nm) or MS detection (*m/z* 500–2000). The amino acid sequences of CVIA and CVIB were cosequenced at a 3:2 ratio,

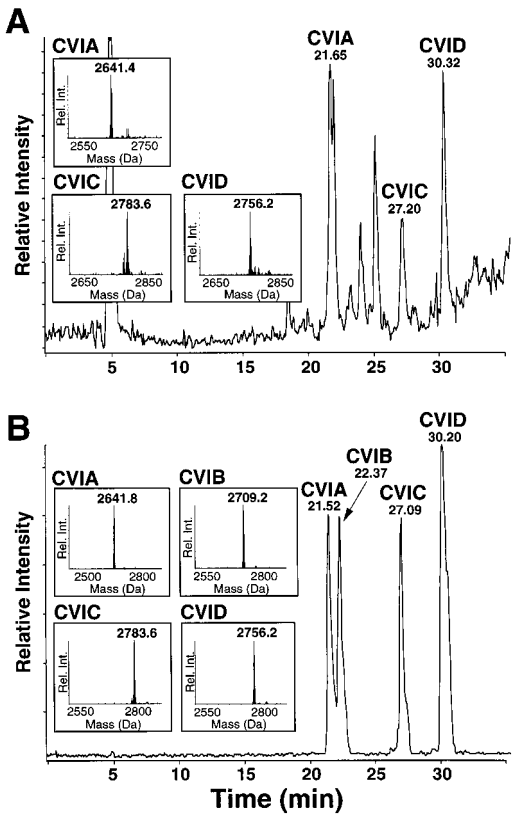

FIG. 1. **HPLC/MS of native and synthetic ω-conotoxins from *C. catus*.** *A*, extracted ion chromatogram of 10 μl of *C. catus* crude venom (*m/z* 800–1400) revealing CVIA, CVIC, and CVID (CVIB was not detected in this batch of crude venom). *B*, extracted ion chromatogram for a mix of synthetic CVIA, CVIB, CVIC, and CVID (*m/z* 800–1400). *Insets* show the reconstructed spectra for CVIA, CVIB, CVIC, and CVID. Retention times and masses for native and synthetic CVIA, CVIC, and CVID were comparable.

whereas CVIC and CVID were obtained from separate fractions. Synthetic C-terminally amidated CVIA, CVIC, and CVID gave retention times and masses that were indistinguishable from the corresponding native peptides (Fig. 1), thus CVIA, CVIC, and CVID were determined to be C-terminally amidated. For each peptide, the oxidized form eluted earlier than the reduced form.

Gene Isolation and Characterization—PCR of the *C. catus* venom duct cDNA templates produced a DNA product of approximately 380–500 base pairs (data not shown). A relatively broad DNA band indicated the presence of a composite PCR product. Subsequent sequence analysis of more than 100 clones derived from the PCR product libraries confirmed this observation. The PCR products contained peptides of the ω- and δ-conotoxin types, as well as sequences from at least two other conotoxin families yet to be assigned. Within the ω-conotoxin sequences isolated were two that translated to putative mature peptides identical to the CVIA and CVID sequences. Despite an extensive screening of the two *C. catus* PCR product libraries, clones for the conotoxins CVIB and CVIC were not located, and the CVID clone was located in only one specimen. The complete nucleotide and predicted amino acid sequences derived for CVIA and CVID are shown in Fig. 2 and are aligned with the sequences for MVIIA and GVIA. Homology screening of public nucleotide and amino acid data bases with the CVIA and CVID sequences indicated that both sequences were unique.

Radioligand Binding—Synthetic CVIA–D, GVIA, MVIIA, and MVIIC each fully displaced ^{125}I-GVIA (defining N-type VSCCs) and ^{125}I-MVIIC (defining P/Q-type VSCCs) binding to crude rat brain membrane (Fig. 3; Table II). GVIA, MVIIA, and

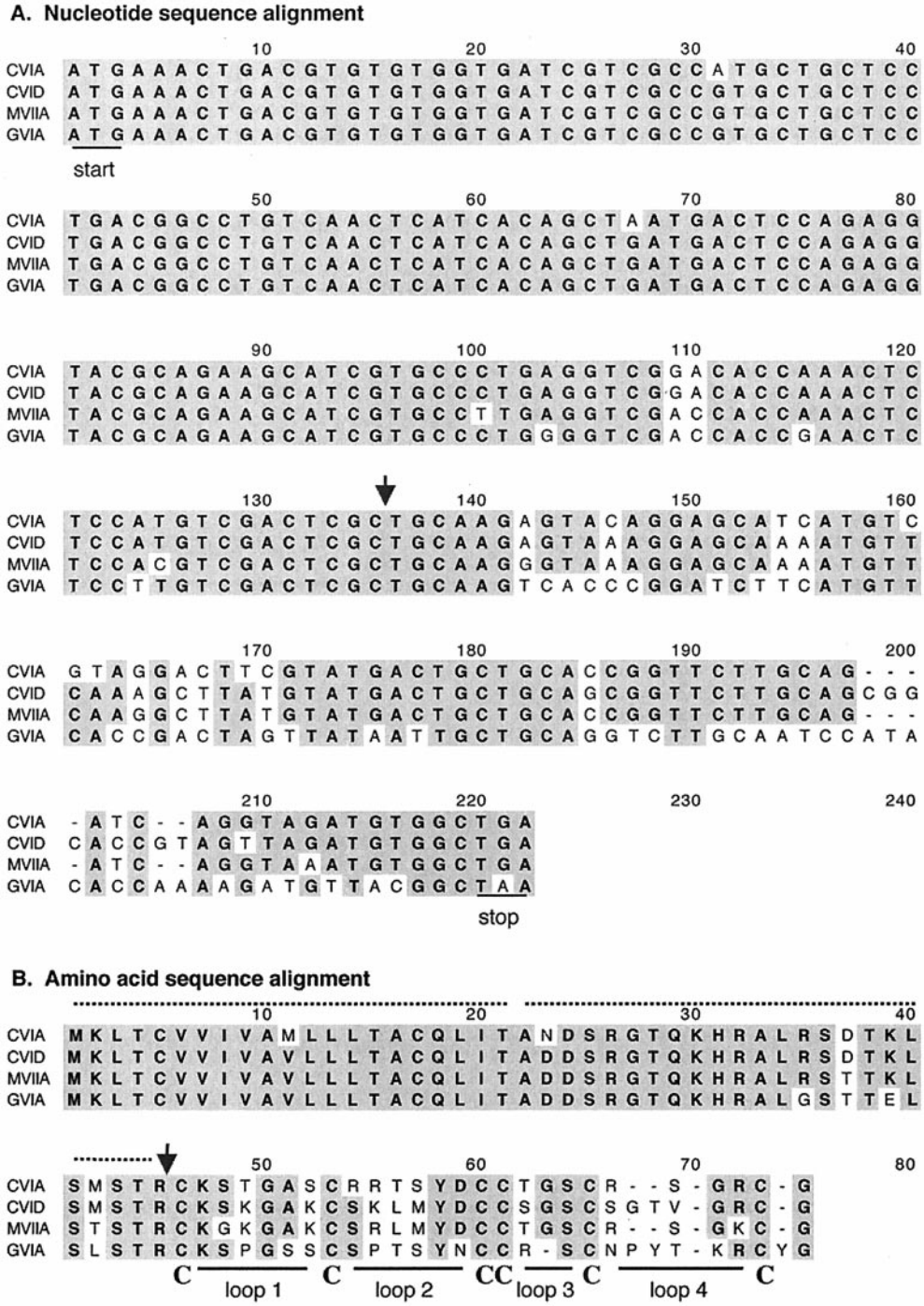

FIG. 2. **Nucleotide and predicted amino acid sequence for the CVIA and CVID peptides.** *A,* ClustalW alignment of nucleotide sequences for the conopeptides CVIA, CVID, GVIA (16), and MVIIA (Australian *C. magus*),[2] with start and stop coding sequences *underlined.* The first 14 residues of CVIA and CVID were generated as part of the PCR primer R-301A. However, subsequent 5′-rapid amplification of cDNA ends PCR indicated that this sequence was identical to the native coding sequence for both peptides (data not shown). The position of the cleavage site between the pre-pro and mature peptide sequences is indicated by an *arrow. B,* ClustalW alignment of the amino acid sequences for the conopeptides CVIA, CVID, MVIIA, and GVIA. The predicted amino acid sequence for MVIIA from *A* was the same as previously reported (55). The predicted signal (positions 1–21) and propeptide (positions 22–45) regions of the leader sequences are highlighted by *dashed lines* (56). An *arrow* indicates the position of the known cleavage site separating the pre-pro and mature peptides of the four sequences. The intercysteine (*C*) loop sequences for the mature peptides are also indicated. Conserved residues are *dark shaded*, and conservative changes in amino acids are *light shaded.*

CVID had similarly high affinity for the N-type VSCC (pIC_{50} ± S.E. values of 10.4 ± 0.05, 10.3 ± 0.03, and 10.2 ± 0.03 M, respectively). In comparison, CVIA was a moderate inhibitor, and CVIB and CVIC were relatively poor inhibitors at the N-type VSCC. GVIA, MVIIA, and CVID also fully displaced ^{125}I-MVIIA, with potencies (IC_{50} values of 49, 29, and 50 pM, respectively) similar to those obtained for displacement of ^{125}I-GVIA. At the P/Q-type VSCC MVIIC had highest affinity (pIC_{50} 9.2 ± 0.04 M); CVIB and CVIC were moderate inhibitors; MVIIA, CVIA, and MVIIA were poor inhibitors; and CVID was an exceptionally weak inhibitor (IC_{50} 55 μM) (Fig. 3*B* and Table II).

Saturation binding studies indicated that ^{125}I-CVID and ^{125}I-MVIIA (67 ± 11 and 37 ± 12 pM, respectively) had poten-

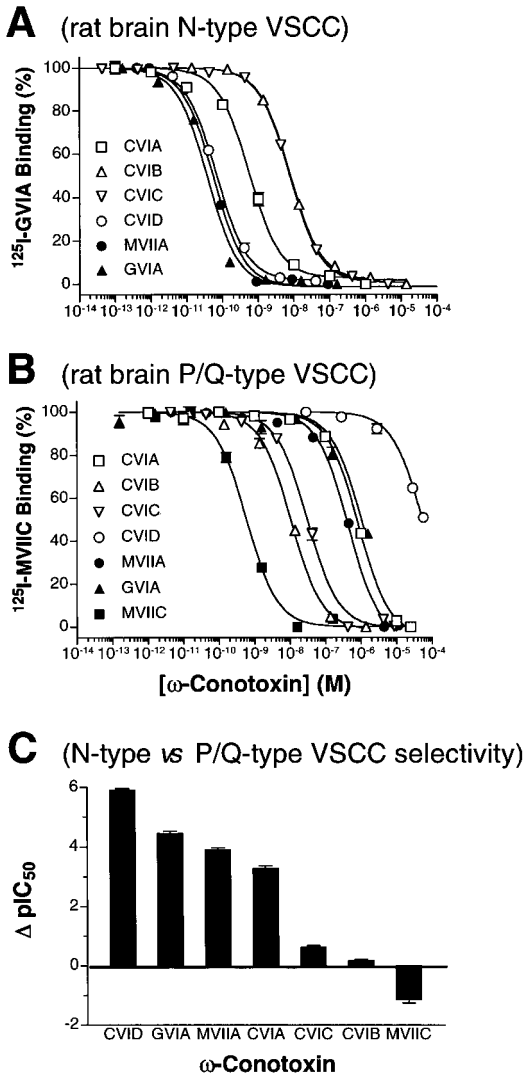

FIG. 3. **ω-Conotoxin potency at N-type and P/Q-type VSCCs in rat brain.** *A,* potency at N-type VSCCs measured by displacement of ^{125}I-GVIA binding. *B,* potency at P/Q-type VSCCs measured by displacement of ^{125}I-MVIIC binding. Displacement data was best fit to a single-site competition model (shown). *C,* selectivity for N-type *versus* P/Q-type VSCCs in rat brain. Shown are the means ± S.E. for pIC_{50} (N-type) and pIC_{50} (P/Q-type).

cies slightly lower than CVID and MVIIA in rat brain membrane, and both appeared to occupy a single class of receptor (Fig. 4). In paired experiments (n = 4), ^{125}I-CVID (0.07 ± 0.03 pmol/mg protein) bound to 31% fewer receptors in rat brain membrane than ^{125}I-MVIIA (0.10 ± 0.04 pmol/mg protein) (p = 0.049, paired two-tailed t test), and ^{125}I-CVID had half the nonspecific binding of ^{125}I-MVIIA (Fig. 4). Despite this difference in the density of receptor sites recognized, displacement assays did not reveal a component of ^{125}I-GVIA or ^{125}I-MVIIA binding that was not displaced by CVID. ^{127}I-CVID (IC_{50} 0.44 nM) also fully displaced ^{125}I-MVIIA binding to rat brain with a Hill slope of unity. However, saturation binding studies have limited power to resolve binding sites of similar affinity, and a lower affinity binding site comprising 30% of receptors would be under-represented with the concentration of ^{125}I-MVIIA used in the displacement assays (20% of its K_d concentration). Displacement of higher concentrations of ^{125}I-MVIIA by MVIIA, GVIA, CVID, or ^{127}I-CVID also did not identify a significant resistant component, possibly due to the reduction in the signal to noise of the assay with increased labeled ligand concentrations (data not shown). The difference in B_{max} did not arise from differences in binding kinetics; ^{125}I-CVID and ^{125}I-MVIIA had similar k_{on} values (0.024 and 0.08 min^{-1} pM^{-1}, after adjusting for k_{off}) and k_{off} values (0.56 and 0.53 min^{-1}, respectively). The K_d values for ^{125}I-CVID and ^{125}I-MVIIA calculated from kinetic data (23 and 7 pM, respectively) were similar to the estimates obtained from saturation binding studies (67 and 37 pM, respectively).

Rat Vas Deferens—CVIA–D inhibited electrically stimulated rat vas deferens contractions (Fig. 5*A*). The rank order of potency was GVIA > CVID ≈ MVIIA > CVIA > CVIC > CVIB (Fig. 5*B* and Table II). Inhibition of the nerve-evoked responses in rat vas deferens was positively correlated with displacement of ^{125}I-GVIA binding across the ω-conotoxins tested (log(rat vas deferens IC_{50}) = 0.78(log(^{125}I-GVIA IC_{50}) + 0.1) (r^2 = 0.92)). CVID and MVIIA gave Hill slopes significantly greater than unity (2.9 and 3.3, respectively), whereas CVIA-C and GVIA gave Hill slopes that were not significantly different from unity. The origin of these differences is unclear; however, differences in N-type *versus* P/Q-type VSCC selectivity do not appear to be a contributing factor. The nonlinear relationship between calcium influx and transmitter release (26) is expected to give rise to a Hill slope greater than unity. Base-line tension was not affected by this series of peptides, and CVID (3×10^{-7} M) had no significant effect on the size of ATP and norepinephrine-induced contractions in rat vas deferens (data not shown, n = 3). A residual component of rat vas deferens contractile activity remained at saturating concentrations of CVID, MVIIA, and GVIA (14.8% (95% CI, 12–18%), 10.5% (7–14%), and 10% (6–14%), respectively) (Fig. 5*B*).

Xenopus Oocytes—Two-electrode voltage clamp studies revealed that CVID and MVIIA were potent inhibitors of ionic currents through peripheral ($\alpha_{1B\text{-}b}$) and central ($\alpha_{1B\text{-}d}$) splice variants of the rat N-type calcium channels expressed in *Xenopus* oocytes in the presence or absence of rat β_3 (Fig. 6; Table III). The voltage dependences of activation of these VSCC conductances were unaffected by CVID or MVIIA (data not shown). CVID and MVIIA had similar potencies to inhibit depolarization-activated inward Ba^{2+} current arising from $\alpha_{1B\text{-}b}$ or $\alpha_{1B\text{-}d}$ coexpressed with rat β_3 (Fig. 6, *C* and *D*). At the $\alpha_{1B\text{-}b}$, the potency of both MVIIA and CVID increased 10-fold in the absence of rat β_3. At the $\alpha_{1B\text{-}d}$, in contrast, CVID potency increased up to 540-fold, whereas MVIIA potency was only slightly increased in the absence of excess rat β_3. Inhibition of the inward Ba^{2+} current by CVID was slowly reversed upon washout, and neither conopeptide inhibited the small endogenous calcium channel current (<5 nA) seen in oocytes that were not injected with cRNA (data not shown). For the α_{1B}/β subunit combinations tested, a relatively small residual N-type current (~10% of maximum peak current) remained in the presence of saturating concentrations of CVID or MVIIA (Fig. 6, *C* and *D*). The residual component had reversal potentials and inward current maxima typical of N-type VSCCs and were completely blocked by bath application of 100 μM Cd^{2+} (data not shown), suggesting that both peptides are unable to occlude completely current through open N-type VSCCs. Further studies are required to confirm that CVID and MVIIA are allosteric inhibitors of the N-type VSCC, as suggested for GVIA from single channel data (27). VSCC chimera studies indicate that GVIA may occlude the pore of the N-type VSCC (28).

^{1}H NMR Studies—The two-dimensional ^{1}H NMR spectra of ω-conotoxins CVIA–D were each assigned using standard protocols (29). As with other ω-conotoxins we have examined (18, 20, 30), peaks were well dispersed, and there was little overlap. CVIA–D secondary shifts closely paralleled those of MVIIA (Fig. 7), whose structure is well defined (30), indicating that the overall fold and disulfide connectivity of these peptides are the

TABLE II
Potency (nM) of ω-conotoxins to inhibit ^{125}I-GVIA (N-type) or ^{125}I-MVIIC (P/Q-type) binding to rat brain VSCCs, and contractions of electrically stimulated rat vas deferens

ω-Conotoxin	Displacement of ^{125}I-GVIA, IC_{50} (95% CI)	Inhibition of vas deferens, IC_{50} (95% CI)	Displacement of ^{125}I-MVIIC, IC_{50} (95% CI)
CVIA	0.56 (0.44–0.70)	205 (170–250)	850 (700–1020)
CVIB	7.7 (7.1–8.5)	630 (480–830)	11 (9.0–13)
CVIC	7.6 (7.0–8.3)	410 (290–590)	31 (26–37)
CVID	0.070 (0.058–0.077)	18.4 (16–21)	55,000 (49,000–62,000)
MVIIA	0.055 (0.047–0.066)	18.2 (15–22)	440 (380–520)
GVIA	0.038 (0.030–0.047)	4.9 (4.0–6.0)	1050 (830–1320)
MVIIC	7.0 (5.3–9.8)		0.60 (0.49–0.72)

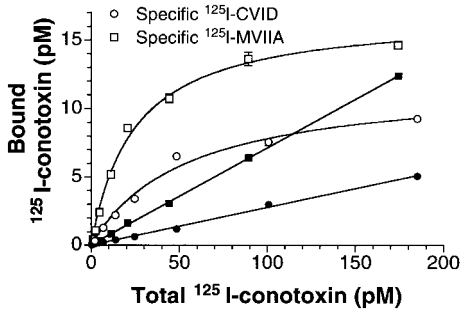

FIG. 4. **Saturation binding of ^{125}I-CVID and ^{125}I-MVIIA to rat brain membrane.** Specific binding (*open symbols*) was best fitted by rectangular hyperbola describing a single binding site. The corresponding *solid symbols* represent nonspecific binding determined in the presence of an excess of the corresponding non-iodinated peptide.

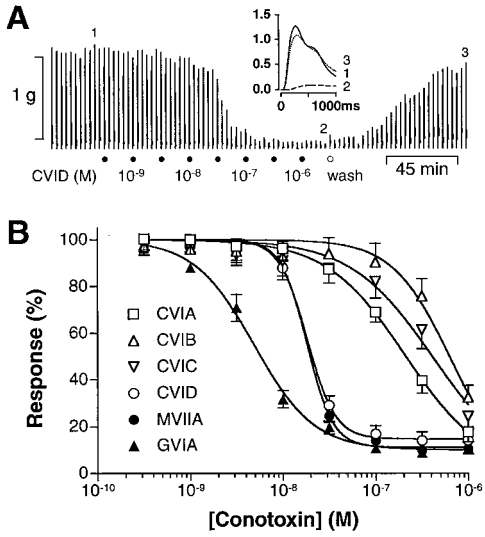

FIG. 5. **ω-Conotoxin inhibition of electrically stimulated rat vas deferens.** *A,* contractile response of guinea pig vas deferens to increasing concentrations of CVID, followed by washout. The *inset* compares single twitch responses recorded before (*1*), during (*2*), and after washout (*3*) of CVID, as indicated. *B,* concentration-dependent inhibition of rat vas deferens twitches by CVIA–D, MVIIA, and GVIA. Note the steep Hill slopes for CVID and MVIIA, and the incomplete inhibition caused by CVID, GVIA, and MVIIA.

same. Secondary Hα shift analysis has been shown to be a sensitive discriminator of disulfide-bonded isomers of other conotoxins (31) and can also be used to identify the location, but not the nature, of local conformational differences across a set of structurally related peptides (32). The secondary Hα shifts of CVIA and CVIB, which have the same loop sizes as MVIIA, are almost identical to those of MVIIA. The secondary Hα shifts of CVIC are also similar to those of MVIIA, apart from loop 4 where the loop sizes are different. In this case, the structure of CVIC would be better approximated by MVIIC, which has the same sized loop 4.

The greatest difference in Hα secondary shifts compared with MVIIA was seen in loops 2 and 4 of CVID. Although differences in loop 4 are not surprising given that CVID has two additional residues, the differences in loop 2 are remarkable given the similarities between MVIIA and CVID at loop 2. The secondary shifts of residues 9–14 in loop 2 of CVID follow the same pattern of those in MVIIA but are of greater magnitude, indicating that the structure of loop 2 in CVID may be more stabilized. This could stem from a long range interaction with loop 4, where the major differences in primary structure are located. Loop 2 has previously been the least defined region of ω-conotoxin structures, with residues of this loop characterized by relatively broad peaks in the ^{1}H NMR spectra, indicative of conformational exchange (30, 33). This lack of structure definition has hindered attempts to understand the crucial role loop 2 plays in activity, function, and selectivity of ω-conotoxins, particularly that of the principal binding determinant Tyr^{13}, as well as residues of secondary importance such as Leu^{11} and Arg^{10} in MVIIA (34). Because no line broadening is observed in loop 2 or elsewhere in CVID but is prominent in loop 2 of MVIIA, CVID may provide a significantly improved structural template for pharmacophore development. Given that the significant differences in secondary Hα shifts for residues in loops 2 and 4 in CVID preclude accurate modeling of CVID from existing ω-conotoxins structures, and given its enhanced N-type selectivity and structural stability, we determined the three-dimensional structure of CVID using ^{1}H NMR spectroscopy, as described below.

Three-dimensional Structure of ω-Conotoxin CVID—CVID structures were calculated based on a total of 481 distance restraints derived from 159 intraresidue, 110 sequential, 184 medium and long range NOEs, 28 hydrogen bond restraints defining a total of 14 hydrogen bonds, and 23 ϕ and 10 $\chi 1$ dihedral angle restraints. A total of 47 of 50 structures converged to a consensus fold, with no NOE distance violation greater than 0.2 Å and no dihedral violations greater than 3°. Of these, the 20 lowest energy structures were chosen to represent the structure of CVID. The structures are exceptionally well defined, with a backbone pairwise root mean squared difference of 0.35 Å (calculated over all residues). The angular order parameters (S) for the ϕ and ψ backbone dihedral angles had average values of 0.99, indicating a high degree of structure precision that is reflected in the low average root mean squared difference to the mean structure of 0.24 Å.

The CVID structures are shown superimposed globally over the backbone atoms, together with the lowest energy structure displayed in secondary structure mode in the same orientation (Fig. 8*A*). The same structures are shown rotated 90°$_y$, to display side chains of residues in loops 2 and 4 which are important for binding (Fig. 8*B*). As for other ω-conotoxins, the secondary structure of CVID is dominated by a triple-stranded β-sheet, in this case incorporating residues 7−9 and 25−27 as the two peripheral strands and residues 19−21 as the central β-strand. Other secondary structural features include a

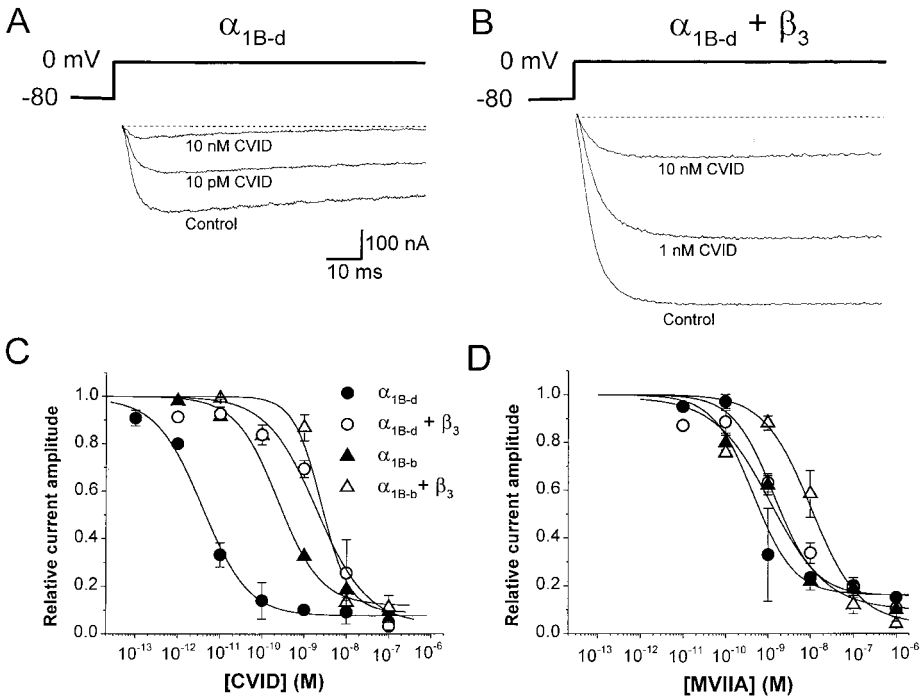

FIG. 6. **CVID and MVIIA inhibition of ionic current arising from the peripheral (α_{1B-b}) and central (α_{1B-d}) splice variants of the rat N-type VSCC expressed in *Xenopus* oocytes.** *A* and *B*, inhibition by CVID of typical depolarization-activated Ba^{2+} currents through α_{1B-d} in the absence (*A*) or presence (*B*) of rat β_3. *C* and *D*, dose-dependent inhibition of peak Ba^{2+} current amplitude through peripheral (*triangles*) and central (*circles*) N-type VSCCs by CVID (*C*) and MVIIA (*D*), in the presence (*open symbols*) and absence (*closed symbols*) of rat β_3.

TABLE III
Potency (nM) of CVID and MVIIA to inhibit Ba^{2+} current through central (α_{1B-d}) and peripheral (α_{1B-b}) splice variants of the rat N-type VSCC in the presence or absence of rat β3 (n = 3–5)

Subunit combination	CVID	MVIIA
α_{1B-d}	0.0037 ± 0.0006	0.45 ± 0.21
α_{1B-d} + β3	2.0 ± 0.7	1.4 ± 0.5
α_{1B-b}	0.23 ± 0.05	1.2 ± 0.6
α_{1B-b} + β3	2.8 ± 0.02	11 ± 6

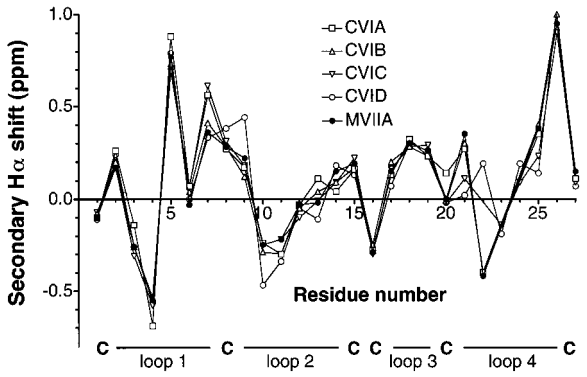

FIG. 7. **Secondary Hα shifts (ppm) for CVIA–D compared with MVIIA.**

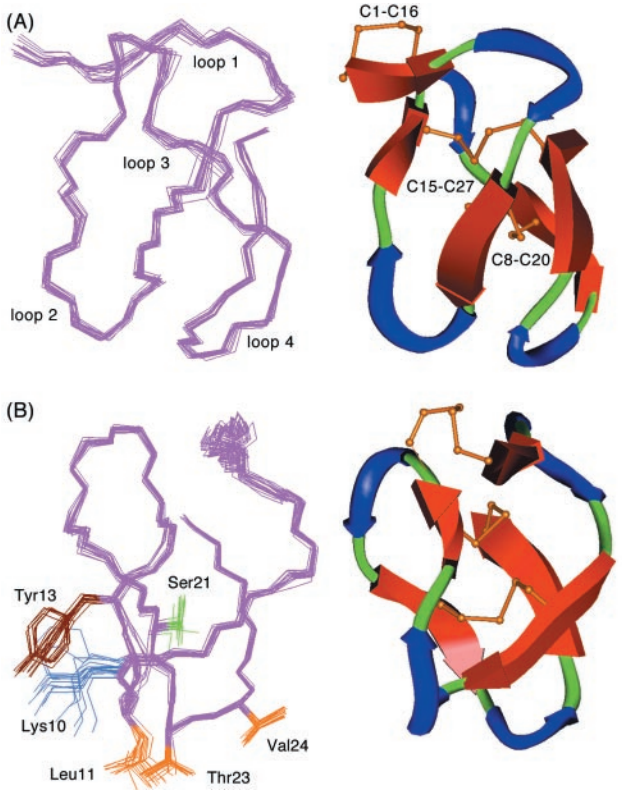

FIG. 8. **The three-dimensional structure of CVID.** *A*, a view of the 20 lowest energy structures of CVID superimposed over the entire backbone, with loops 1–4 indicated. Adjacent is one structure shown in the same orientation highlighting the β-bridge and sheets (*red arrows*), the turns (*blue arrows*), and the location of disulfide bridges (*ball-and-stick*). *B*, structures in *A* rotated 90°$_y$, showing the positions of side chains of residues in loops 2 and 4 that may contribute to the activity of CVID at N-type VSCCs, including a new interaction through Val^{24}.[2]

β-bridge composed of residues 1−2 and 14−16 and several β-turns. The β-turns that link the β-sheet and β-bridge regions comprise residues 3−6 (type II), 9−12 (type I), 10−13 (type I), 15−18 (type I), and 21−24 (type IV). The β-bridge has not previously been reported explicitly for other ω-conotoxins but is likely to exist in MVIIA, GVIA, and MVIIC and has been identified in κ-conotoxin PVIIA, which adopts the same structure as the ω-conotoxins but targets the *Shaker* potassium channel (35). Structural features of CVID that have not been described for other ω-conotoxins are the presence of two hydrogen bonds from the NH protons of Lys^{10} and Leu^{11} to the C=O oxygen atoms of Gly^{22} and Thr^{23}, respectively. It is likely that these enhance the stability of loop 2 in CVID compared with other ω-conotoxins. Importantly, the backbone of Tyr^{13} is stabilized in the α_L conformation, with the $\chi 1$ side chain torsion angle at −60°. NMR data confirming this conformation for Tyr^{13} in CVID include the presence of a strong intraresidue NH_i-$H\alpha_i$ NOE, together with a weaker $H\alpha_{i-1}$-NH_i and a $^3J_{NH-H\alpha}$ coupling constant of 7 Hz (36). Attempts to define the conformation of Tyr^{13} in other ω-conotoxins have been ambig-

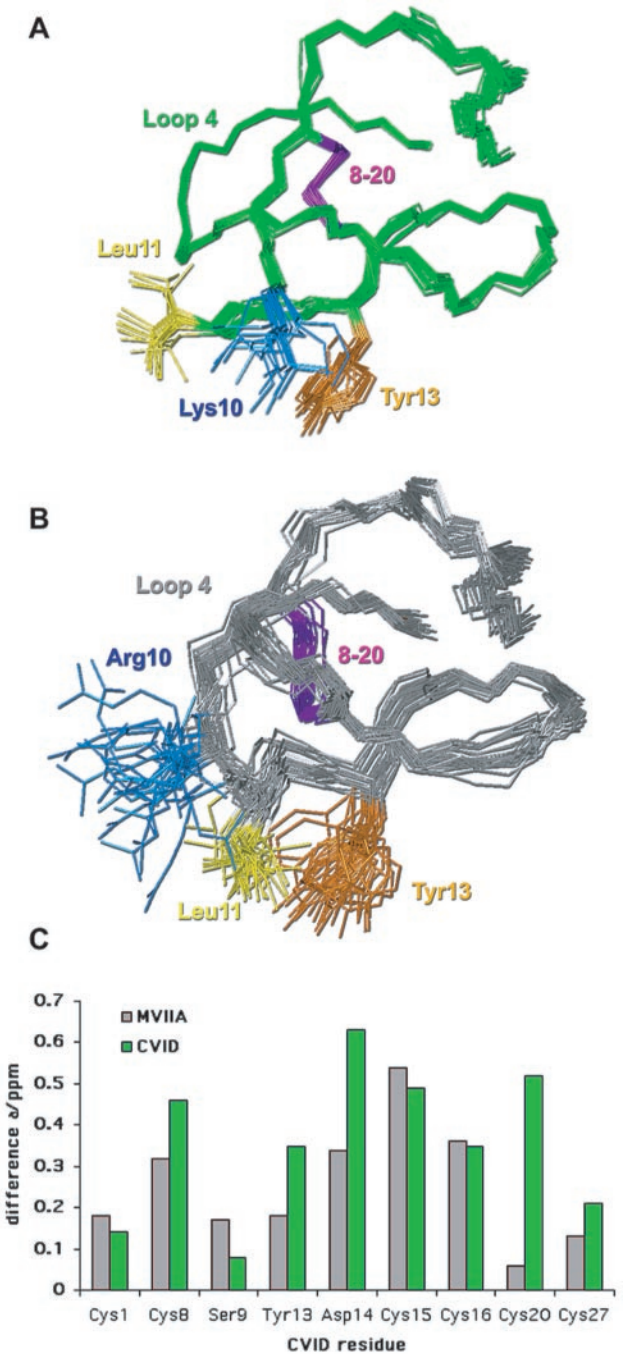

FIG. 9. **Comparison of CVID and MVIIA (55) structures.** Shown in the same global orientation are the backbone superimposition of the 20 lowest energy structures of CVID (*green*) (*A*), and a set of 34 structures of MVIIA (*gray backbone*, Protein Data Bank code *1DW5*, see Ref. 55) comprising both $\chi 3$ families that were calculated with a force constant of 40 kcal/mol applied to the three disulfide bridge dihedral angles $C\beta_i$–$S\gamma_i$–$S\gamma_j$–$C\beta_j$ (*B*). The disulfide bridge Cys^8–Cys^{20} (*purple*), and the side chains of important binding residues Arg^{10} (Lys^{10} in CVID) (*blue*), Leu^{11} (*yellow*), and Tyr^{13} (*orange*) are identified. The position of loop 4 is indicated in *A* and *B*. *C* shows a comparison of differences in Hβ shifts for selected residues of CVID (*green*) and MVIIA (*gray,* 30). Note that CVID has greater separations of Hβ shifts, particularly at Cys^8, Tyr^{13}, Asp^{14}, and Cys^{20}.

uous, and indeed Tyr^{13} may adopt an averaged conformation in other ω-conotoxins. The enhanced structural stability of CVID is further reinforced by a comparison of the Hβ shifts of CVID and MVIIA (Fig. 9*C*). The Hβ protons of Cys^{20} are degenerate in MVIIA indicative of disulfide bond isomerization, whereas the corresponding protons in CVID have disparate shifts indicative of an absence of any disulfide bond isomerization. The Hβ shifts differences of Cys^8, Tyr^{13}, and Asp^{14} are also significantly greater in CVID than in MVIIA. This trend is followed over the temperature range 280–298 and the pH range 3–6 (data not shown).

DISCUSSION

By using assay-directed fractionation, we have isolated four new ω-conotoxins from *C. catus*, named ω-conotoxins CVIA–D. These four conotoxins were chemically synthesized and folded to be indistinguishable from the native peptides. *C. catus* is the sixth piscivorous cone snail to evolve mammalian active ω-conotoxins for prey capture. Analogous to other ω-conotoxins identified to date, CVIA–D have three disulfide bonds, fall within the mass range 2500–3600 Da (4), and are relatively hydrophilic. Inspection of the sequences in Table I reveals a conserved cysteine framework and three conserved residues Gly^5, Tyr^{13}, and Ser^{19} (CVID numbering) among ω-conotoxins. Homology at loops 1–4 varies from 0 to 60% sequence identity among these ω-conotoxins, with the largest difference occurring in loop 4 of CVID. Cloning and sequencing of mRNA transcripts from the venom ducts of two specimens of *C. catus* confirmed CVIA and CVID are expressed in this tissue. Our inability to isolate mRNA transcripts encoding CVIB and CVIC was most likely associated with the relatively low abundance of these peptides. Variation in the levels of specific peptides between individual *C. catus* could also be involved.[2] Isolation of cDNA templates for CVIB and CVIC may require the analysis of additional *C. catus* specimens or the use of additional "PCR markers" that are more specific for the mature peptide sequences.

CVIA–D each fully displaced ^{125}I-GVIA and ^{125}I-MVIIC binding to rat brain membrane. CVID, GVIA, and MVIIA were similarly potent at rat brain N-type VSCCs. However, CVID was 100-fold more selective than MVIIA for N-type over P/Q-type VSCCs, and ^{125}I-CVID bound to 30% fewer sites in rat brain membrane than ^{125}I-MVIIA. Similar differences in B_{max} were not observed in saturation binding of ^{125}I-CVID and ^{125}I-MVIIA to human brain membrane, suggesting that pharmacological differences exist in the N-type VSCCs present in rat and human brain. Further studies are required to determine the origin of these differences. CVIA–D were reversible inhibitors of peripheral N-type VSCCs involved in neurally evoked transmitter release in rat vas deferens. Inhibition of neurotransmitter release was positively correlated with the displacement of ^{125}I-GVIA binding, consistent with N-type VSCCs being the major source of Ca^{2+} influx contributing to neurotransmitter release in the rat vas deferens stimulated at low frequencies (37–40). A correlation between inhibition of Ca^{2+} influx and ligand displacement at the N-type VSCC was shown for a series of MVIIA and TVIA analogues (41) but not for a series of GVIA analogues (33). Potency estimates obtained using the vas deferens were lower than estimates obtained from radioligand displacement studies (Table II), consistent with previous observations (37, 42). The relatively high levels of Ca^{2+} in the physiological solution for the vas deferens compared with the binding assays is likely to contribute to this difference in potency, since Ca^{2+} is a non-competitive inhibitor of ω-conotoxin binding (13). CVID had no effect on contractions of the vas deferens induced by exogenously applied ATP or norepinephrine or on voltage-sensitive sodium channels in rat autonomic neurons.[2]

In *Xenopus* oocytes, CVID and MVIIA inhibited the inward current through central ($\alpha_{1B\text{-}d}$) and peripheral ($\alpha_{1B\text{-}b}$) splice variants of the rat N-type VSCC. In the presence of rat β_3 subunit, chosen because it assembles with α_{1B} (43) and is widely distributed in rat brain (44), MVIIA and CVID had

similar potencies. However, the potency of MVIIA and CVID increased at $\alpha_{1B\text{-}d}$ and $\alpha_{1B\text{-}b}$ expressed in the absence of rat β_3. This increase was most pronounced for CVID at $\alpha_{1B\text{-}d}$ (up to 540-fold), intermediate for CVID and MVIIA at $\alpha_{1B\text{-}b}$ (~10-fold), and least pronounced for MVIIA at $\alpha_{1B\text{-}d}$ (3-fold). Previous studies have shown that the β subunit can influence the affinity of local anesthetics (45) and spider toxins (46) for α_{1A} (P/Q-type) calcium channels expressed in oocytes and mammalian cells. Oocytes express low levels of an endogenous β subunit (β_{3xo}) with high homology to rat β_3 that is essential for expression of functional channels, and overexpression of either of these β_3 subunits causes the same facilitation of VSCC current activation and inactivation (47). We propose that expression of excess β_3 can differentially modify ω-conotoxin pharmacology at central and peripheral splice variants of the N-type VSCC, presumably by binding to an intracellular domain of α_{1B} to cause an extracellular conformational change that reduces ω-conotoxin binding.

The alternatively spliced $\alpha_{1B\text{-}d}$ and $\alpha_{1B\text{-}b}$ differ at extracellular loops IIIS3-S4 (+SFMG and −SFMG, respectively) and IVS3-S4 (−ET and + ET, respectively), indicating that relatively small changes in the sequence of α_{1B} not only influence channel kinetics (insertion of ET in $\alpha_{1B\text{-}b}$ slows activation kinetics (48)), but modify ω-conotoxin pharmacology. Since ω-conotoxins bind preferentially to the inactivated state than the resting state of N-type calcium channels (49), the observed effect is not through excess β subunit that would act to increase the proportion of channels in the inactivated state (47). This auxiliary subunit effect may occur through the action of excess β subunit at a second site that is present at the C terminus of α_{1A}, α_{1B}, and α_{1E} (50), but a differential effect of rat and *Xenopus* β_3 on the pharmacology of ω-conotoxins may also be involved. The potency of Aga IVA and funnel web spider toxin were reduced ~10-fold when α_{1A} was coexpressed in mammalian cells with β_3 or β2, rather than with β1b (46). The extent to which ω-conotoxin pharmacology at central and peripheral splice variants of α_{1B} is influenced by different combinations of the five α2/δ subunits and the four β subunits requires further investigation, given the heterogeneity of α_{1B}/auxiliary subunit combinations in the brain (43). The differential effect of β subunits on ω-conotoxin pharmacology at central and peripheral splice variants of α_{1B} may lead to the development of ω-conotoxins with selectivity for specific forms of the N-type VSCC present in different neural pathways. However, the precise location of specific combinations of α_{1B} splice variants and different β subunits have not yet been determined.

The ability of CVID to discriminate among different forms of the N-type VSCC may also have therapeutic implications. In a Freund's complete adjuvant model of inflammatory pain in rats, chronic intrathecal administration of CVID (AM336; 0.36 nmol/h) produced sustained antinociception with mild behavioral side effects (mean scores 0.5–1 on a scale of 7) over a 7-day infusion period. In comparison, MVIIA (Ziconotide; 0.1 for first 24 h and 0.13 nmol/h for next 6 days) produced similar initial levels of antinociception that returned to base line by day 6, whereas levels of motor side effects (mean scores 3–4) were greater and maintained throughout the 7-day infusion period (52).[3] These effects of MVIIA and CVID were completely reversed on ceasing conotoxin infusion. CVID has recently gained approval to enter clinical trials for the treatment of severe pain.

^{1}H NMR studies reveal that CVID adopts a unique fold, with loop 4 curved toward loop 2 to create a globular surface. In contrast, loop 4 is oriented parallel to loop 2 in MVIIA and MVIIC and away from loop 2 in GVIA (18, 30, 53, 54). The presence of two hydrogen bonds between loops 2 and 4 in CVID favor loop 4 in this orientation, whereas hydrogen bonds between loops 2 and 4 have not been reported previously for GVIA, MVIIA or MVIIA. Early structural studies on MVIIA (30) raised the possibility of loop 2 instability, based on the observation of broadened lines in this region. This was supported by a recent study on the dynamics of MVIIA (55), where it was suggested that the motion of loop 2 was facilitated by isomerization of the disulfide bridge between Cys^8 and Cys^{20}. In that study, the introduction of a force constant of 40 kcal mol^{-1} into the empirical force field restrained the χ3 angle of this disulfide bridge to ±90° resulting in two closely related families of structures (55). No such isomerization is evident in CVID, where a corresponding force constant of only 10 kcal/mol yielded a conformation of +90° in all structures. In addition, the χ1 angles at Cys^{20} for MVIIA (+180°) and CVID (−60°) differed significantly, as do the magnitude of $H\beta_2/H\beta_3$ shift differences of AM*X* residues (Fig. 9*C*). The greater Hβ shift differences of Cys^8, Cys^{20}, Tyr^{13}, and Asp^{14} in CVID indicate that the side chains of these residues undergo less conformational exchange than MVIIA. The improved stability of this disulfide bridge in CVID together with the interloop hydrogen bonds may act to restrain loop 2 motion, providing an entropic advantage for binding. This overall stability of CVID is also likely to contribute to its selectivity, since loop 2/4 combinations contain many of the primary determinants for ω-conotoxin selectivity between N-type and P/Q-type VSCCs (18).

CVID and two closely related families of MVIIA (55) structures are compared to highlight important differences in the orientation of loops 4 and 2 (Fig. 9). Although Tyr^{13} occupies similar spatial positions, the positions of the side chains of the important binding residues 10 and 11 appear reversed in the two peptides. According to Atkinson *et al.* (55), motion in MVIIA results in time-averaged NOEs that ultimately produce flaws in the resulting structure. Such motion does not appear to be present in CVID, since no line broadening is observed in loop 2 or elsewhere in the peptide. This, together with the increased number of distance restraints, particularly in the loop 2 region, ensures that the structure of CVID is represented by a single, well defined conformation. Interestingly, CVID lacks the secondary binding residues present in loop 4 of MVIIA (Arg^{21}) (34) or GVIA (Lys^{24} and Tyr^{22}) (33) but utilizes a new ω-conotoxin/VSCC interaction through the relatively exposed Val^{24}.[2] These structural features presumably act in concert to influence the selectivity of CVID, as well as providing a well defined template for pharmacophore development and the design of peptidomimetic inhibitors of N-type VSCCs.

Acknowledgments—We thank Alan Robertson (AMRAD Operations Pty Ltd.) for support and advice during this study and constructive comments on the manuscript. We also thank Roger Moni for assistance performing radioligand binding studies and Diane Lipscombe (Brown University, Providence, RI) for providing the DNA encoding the rat $\alpha_{1B\text{-}b}$, $\alpha_{1B\text{-}d}$, and β_3 clones. A specimen of *C. catus* has been lodged at the Australian Museum (registration number C.352495).

REFERENCES

1. Adams, D. J., Alewood, P. F., Craik, D. J., Drinkwater, R., and Lewis, R. J. (1999) *Drug Dev. Res.* **46,** 219–234
2. Olivera, B. M., Gray, W. R., Zeikus, R., McIntosh, J. M., and Varga, J. (1990) *Science* **230,** 1338-1343
3. McIntosh, J. M., Olivera, B. M., and Cruz, L. J. (1999) *Methods Enzymol.* **294,** 605–624
4. Miljanich, G. P., and Ramachandran, J. (1995) *Annu. Rev. Pharmacol. Toxicol.* **35,** 707–734
5. Seabrook, G. R., and Adams, D. J. (1989) *Br. J. Pharmacol.* **97,** 1125-1136
6. Takahashi, T., and Momiyama, A. (1993) *Nature* **366,** 156-158
7. McDonough, S. I., Swartz, K. J., Mintz, I. M., Boland, L. M., and Bean, B. P. (1996) *J. Neurosci.* **16,** 2612-2623
8. Currie, K. P., and Fox, A. P. (1997) *J. Neurosci.* **17,** 4570-4579
9. Yamada, K., Teraoka, T., Morita, S., Hasegawa, T., and Nabeshima, T. (1994) *Neuropharmacology* **33,** 251-254

[3] M. Smith, personal communication.

10. Malmberg, A. B., and Yaksh, T. L. (1995) *Pain* **60,** 83-90
11. Wetenbroek, R. E., Hoskins, L., and Catterall, W. A. (1998) *J. Neurosci.* **18,** 6319-6330
12. Penn, R. D., and Paice, J. (2000) *Pain* **85,** 291–296
13. Kristipati, R., Nádasdi, L. Tarczy-Hornoch, K., Lau, K., Miljanich, G. P., Ramachandran, J., and Bell, J. R. (1994) *Mol. Cell. Neurosci.* **5,** 219-228
14. Lin, Z., Haus, S., Edgerton, J., and Lipscombe, D. (1997) *Neuron* **18,** 153–166
15. Woodward, S. R., Cruz, L. J., Olivera, B. M., and Hillyard, D. R. (1990) *EMBO J.* **9,** 1015–1020
16. Colledge, C. J., Hunsperger, J. P., Imperial, J. S., and Hillyard, D. R. (1992) *Toxicon* **30,** 1111–1116
17. Schnölzer, M., Alewood, P., Jones, A., Alewood, D., and Kent, S. B. H. (1992) *Int. J. Pept. Protein Res.* **40,** 180-193
18. Nielsen, K. J., Adams, D., Thomas, L., Bond, T. J., Alewood, P. F., Craik D. J., and Lewis, R. J. (1999) *J. Mol. Biol.* **289,** 1405-1421
19. Bidlingmeyer, B. A., Cohen, S. A., and Tarvin, T. L. (1984) *J. Chromatogr.* **336,** 93-104
20. Nielsen, K. J., Adams, D. A., Alewood, P. F., Lewis, R. J., Thomas, L., Schroeder, T., and Craik, D. J. (1999) *Biochemistry* **38,** 6741-6751
21. Cruz, L. J., and Olivera, B. M. (1986) *J. Biol. Chem.* **261,** 6230-6233
22. Brünger, A. T., Clore, G. M., Gronenborn, A. M, and Karplus, M. (1986) *Proc. Nat. Acad. Sci. U. S. A.* **83,** 3801-3805
23. Brünger, A. T. (1992) *A System for X-ray Crystallography and NMR,* X-PLOR Version 3.1, Yale University, New Haven
24. Rice, L. M., and Brünger, A. T. (1994) *Proteins Struct. Funct. Genet.* **19,** 277–290
25. Stein, E. G., Rice, L. M., and Brünger, A. T. (1996) *J. Magn. Reson.* **124,** 1554–1564
26. Wheeler, D. B., Randall, A., and Tsien, R. W. (1996) *J. Neurosci.* **16,** 2226–2237
27. Witcher, D. R., De Waard, M., and Campbell, K. P. (1993) *Neuropharmacology* **32,** 1127–1139
28. Ellinor, P. T., Zhang, J.-F., Horne, W. A., and Tsien, R. W. (1994) *Nature* **372,** 272–275
29. Wüthrich, K. (1986) *NMR of Proteins and Nucleic Acids,* pp. 1–292, Wiley-Interscience, New York
30. Nielsen, K. J., Thomas, L., Lewis, R. J., Alewood, P. F., and Craik., D. J. (1996) *J. Mol. Biol.* **263,** 297-310
31. Gehrmann, J., Alewood, P., and Craik, D. (1998) *J. Mol. Biol.* **278,** 401-415
32. Nielsen, K. J., Skjærbæk, N., Dooley, M., Adams, D. A., Mortensen, M., Dodd, P., Craik, D. J., Alewood, P. F., and Lewis, R. J. (1999) *J. Med. Chem.* **42,** 415-426
33. Lew, M. J., Flinn, J. P., Pallaghy, P. K., Murphy, R., Whorlow, S. L., Wright, C. E., Norton, R. S., and Angus, J. A. (1997) *J. Biol. Chem.* **272,** 12014-12023
34. Nadasdi, L., Yamashiro, D., Chung, D., Tarczyhornoch, K., Adriaenssens, P., and Ramachandran, J. (1995) *Biochemistry* **34,** 8076-8081
35. Scanlon, M. J., Naranjo, D., Thomas, L., Alewood, P. F., Lewis, R. J., and Craik, D. J. (1997) *Structure* **5,** 1585-1597
36. Ludrigsen, S., and Poulsen, F. M. (1992) *J. Biomol. NMR* **2,** 227-233
37. Boot, J. R. (1994) *Eur. J. Pharmacol.* **258,** 155-158
38. Maggi, C. A., Patacchini, R., Santicioli, P., Lippe, I. Th, Giuliani, S., Geppetti, P., Del Bianco, E., Selleri, S., and Meli, A. (1988) *Naunyn-Schmiedeberg's Arch. Pharmacol.* **338,** 107-113
39. Smith, A. B., and Cunnane, T. (1996) *Neuroscience* **70,** 817-824
40. Wright, C. E., and Angus, J. A. (1996) *Br. J. Pharmacol.* **118,** 49-56
41. Wang, Y.-X., Bezprozvannaya, S., Bowersox, S. S., Nadasdi, L., Miljanich, G., Mezo, G., Silva, D., Tarczy-Hornoch, K., and Luther, R. R. (1998) *Naunyn-Schmiedeberg's Arch. Pharmacol.* **357,** 159–168
42. Flinn, J. P., Pallaghy, P. K., Lew, M. J., Murphy, R., Angus, J. A., Norton, R. S. (1999) *Eur. J. Biochem.* **262,** 447–455
43. Scott, V. E., De Waard, M., Liu, H., Gurnett, C. A., Venzke, D. P., Lennon, V. A., and Campbell, K. P. (1996) *J. Biol. Chem.* **271,** 3207–3212
44. Ludwig, A., Flockerzi, V., and Hofmann, F. (1997) *J. Neurosci.* **17,** 1339–1349
45. Zamponi, G. W., Soong, T. W., Bourinet, E., and Snutch, T. P. (1996) *J. Neurosci.* **16,** 2430–2443
46. Moreno, H., Rudy, B., and Llinás, R. (1997) *Proc. Natl. Acad. Sci. U. S. A.* **94,** 14042–14047
47. Tareilus, E., Roux, M., Qin, N., Olcese, R., Zhou, J., Stefani, E., and Birnbaumer, L. (1997) *Proc. Natl. Acad. Sci. U. S. A.* **94,** 1703-1708
48. Lin, Z., Lin, Y., Schorge, S., Pan, J. Q., Beierlein, M., and Lipscombe, D. (1999) *J. Neurosci.* **19,** 5322-5331
49. Stocker, J. W., Nadasdi, L., Aldrich, R. W., and Tsein, R. W. (1997) *J. Neurosci.* **17,** 3002–3013
50. Birnbaumer, L., Qin, N., Olcese, R., Tareilus, E., Platano, D., Costantin, J., and Stefani, E. (1998) *J. Bioenerg. Biomembr.* **30,** 357-375
51. Ramilo, C. A., Zafaralla, G. C., Nadasdi, L., Hammerland, L. G., Gray, W. R., Krispati, R., Ramachandran, J., Miljanich, G., Olivera, B. M., and Cruz, L. J. (1992) *Biochemistry* **31,** 9919–9926
52. Smith, M. T., Ross, F. B., Lewis, R., Kurek, J. B., and Cabot, P. J. (2000) *Aust. Soc. Clin. Exp. Pharm. Toxicol.* **7,** 50
53. Davis, J. H., Bradley, E. K., Miljanich, G. P., Nadasdi, L., Ramachandran, J., and Basus, V. J. (1993) *Biochemistry* **32,** 7396-7405
54. Nielsen, K. J., Schroeder, T., and Lewis, R. (2000) *J. Mol. Recognit.* **13,** 55–70
55. Atkinson, R. A., Kieffer, B., Dejaegere, A., Sirockin, F., and Lefevre, J. F. (2000) *Biochemistry* **39,** 3908–3919
56. Price-Carter, M., Gray, W. R., and Goldenberg, D. P. (1996) *Biochemistry* **35,** 15547–15557
57. Olivera, B. M., McIntosh, J. M., Cruz, L. J., Luque, F. A., and Gray, W. R. (1984) *Biochemistry* **23,** 5087-5090
58. Olivera, B. M., Cruz, L. J., deSantos, V., LeChaminant, G. W., Griffin, D., Zeikus, R., McIntosh, J. M., Galyean, R., Varga, J., Gray, W. R., and Rivier, J. (1987) *Biochemistry* **26,** 2086–2090
59. Hillyard, D. R., Monje, V. D., Mintz, I. M., Bean, B. P., Nadasdi, L., Ramachandran, J., Miljanich, G., Azimi-Zonooz, A., McIntosh, J. M., Cruz, L. J., Imperial, J. S., and Olivera, B. M. (1992) *Neuron* **9,** 69–77